Analytica Chimica Acta 753 (2012) 32–41

Contents lists available at SciVerse ScienceDirect

Analytica Chimica Acta

journal homepage: www.elsevier.com/locate/aca

Layer by layer assembly of catalase and amine-terminated ionic liquid onto titanium nitride nanoparticles modified glassy carbon electrode: Study of direct voltammetry and bioelectrocatalytic activity

Shagayegh Saadati [a], Abdollah Salimi [a,b,*], Rahman Hallaj [a], Amin Rostami [a]

[a] Department of Chemistry, University of Kurdistan, P.O. Box 416, Sanandaj, Iran
[b] Research Center for Nanotechnology, University of Kurdistan, P.O. Box 416, Sanandaj, Iran

HIGHLIGHTS

- Catalase and amine-terminated ionic liquid were immobilized to GC/TiNnp with LBL assembly method.
- First a thin layer of NH_2-IL is covalently attached to GC/TiNnp electrode using electro-oxidation.
- With alternative assemble of IL and catalase with positive and negative charged, multilayer was formed.
- Immobilized catalase shows excellent electrocatalytic activity toward H_2O_2 reduction.
- Biosensor response is directly correlated to the number of bilayers.

GRAPHICAL ABSTRACT

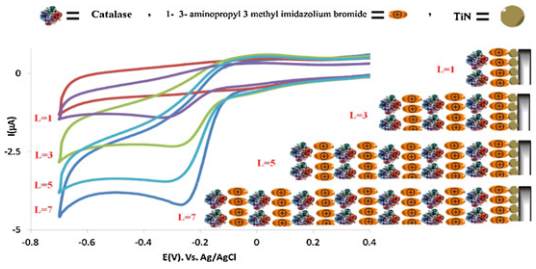

ARTICLE INFO

Article history:
Received 5 July 2012
Received in revised form
23 September 2012
Accepted 25 September 2012
Available online 2 October 2012

Keywords:
Layer by layer
Catalase
IL
Titanium nitride nanoparticle
H_2O_2
Biosensor

ABSTRACT

A novel, simple and facile layer by layer (LBL) approach is used for modification of glassy carbon (GC) electrode with multilayer of catalase and nanocomposite containing 1-(3-Aminopropyl)-3-methylimidazolium bromide (amine terminated ionic liquid (NH_2-IL)) and titanium nitride nanoparticles (TiNnp). First a thin layer of NH_2-IL is covalently attached to GC/TiNnp electrode using electro-oxidation method. Then, with alternative self assemble positively charged NH_2-IL and negatively charged catalase a sensitive H_2O_2 biosensor is constructed, whose response is directly correlated to the number of bilayers. The surface coverage of active catalase per bilayer, heterogeneous electron transfer rate constant (k_s) and Michaelis–Menten constant (K_M) of immobilized catalase were 3.32×10^{-12} mol cm^{-2}, 5.28 s^{-1} and 1.1 mM, respectively. The biosensor shows good stability, high reproducibility, long life-time, and fast amperometric response with the high sensitivity of 380 μA mM^{-1} cm^{-2} and low detection limit of 100 nM at concentration range up to 2.1 mM.

1. Introduction

The direct electron transfer between redox proteins/enzymes and the electrode surface has received considerable attention recently, because it can provide information about the electron transfer mechanism of proteins in biological systems and bio-fuel cells. Furthermore, it is also used in fabricating the third generation

* Corresponding author at: Department of Chemistry, University of Kurdistan, P.O. Box 416, Sanandaj, Iran. Tel.: +98 8716624001; fax: +98 8716624008.
E-mail addresses: absalimi@uok.ac.ir, absalimi@yahoo.com (A. Salimi).

0003-2670/$ – see front matter © 2012 Elsevier B.V. All rights reserved.
http://dx.doi.org/10.1016/j.aca.2012.09.043

biosensors and bioelectronics devices [1]. Since redox centers are deeply buried within the proteins molecules, the electron transfer between proteins and the electrode is difficult. Therefore, many substrates were used to immobilize redox enzymes or proteins on the electrode surfaces. Due to the poor adsorptive capacity of enzymes onto the electrode surface, the selection of the immobilization technique and supported matrix is the key step in the direct electron transfer kinetics of redox enzymes or proteins. In recent years, various methodologies such as physical adsorption, covalent attachment, layer-by-layer (LBL) assembly technique, entrapment and encapsulation have been developed for the immobilization of enzymes on a suitable matrix for construction of biosensors [2,3].

Among various methods that have been used for immobilization of enzymes, LBL technique has attracted much attention because of its simplicity in the procedure, precise control of film composition, thickness, roughness and porosity, and employing numerous different materials in the fabrication of films [4–6]. Therefore, the LBL method has received considerable attention in the field of electrochemistry as a promising tool for the fabrication of nanostructures films with high organization at the nanoscale level and their application in sensors and biosensors field [7,8]. This technique involves an alternate adsorption of enzyme and electrolyte from solution onto an electrode surface through electrostatic adsorption [9,10] or covalent bond formation [11–13]. Biocompatible materials have long attracted increasing attention worldwide because of their desirable properties and potential applications in biomedicine [14], biosensor [15], biocatalysis [16] and bioelectronics [17]. Biocompatible nanomaterials can provide a favorable environment for redox proteins and enzymes to realize direct electrochemistry and to fabricate excellent biosensors and as a model for understanding complex electron-transfer mechanisms in biological systems [18].

In recent years ionic liquids (ILs) have been used in the field of electrochemistry and electroanalysis due to their unique physicochemical properties including higher ionic conductivity, wider electrochemical windows, negligible vapor pressure, higher chemical and thermal stability, good antifouling ability and good biocompatibility [19–22]. ILs can serve not only as the supporting electrolyte in the electrochemical process [23] but also as the modifier in the chemically modified electrodes [24]. ILs-based electrochemical sensors and biosensors have been extensively reported for the direct electron transfer of various redox enzymes [25,26] and detection of different compounds such as ascorbic acid [27], dopamine [28], H_2O_2 [24], glucose [29], oxygen [21] and nitrite [30].

The nanocomposites containing IL and different nanomaterials such as gold nanoparticles [31], gold nanorods [32], carbon nanotubes [33,34], carbon nanofibers [35], graphene nanosheets [36], Fe_2O_3 nanoparticles [37], CdS nanorods [38], TiO_2-graphene nanocomposites [21] and CNTs-gold nanoparticles [39] were used for the fabrication of the third generation of biosensors.

Titanium nitride (TiN) with physical, chemical, mechanical, and electrical properties such as high degree of hardness, chemical stability, high thermal conductivity, chemical inertness and biocompatibility has been used in various fields, such as pH sensitive material [41], electrode for stripping voltammmetry measurement [42] electroanalytical applications [40], high surface area material for catalytic processes [43], hydrogen storage, and supercapacitors [44]. However, it has not been reported the direct electrochemistry of immobilized catalase onto TiNnp/IL nanocomposite system.

Amperometric H_2O_2 biosensors based on immobilization of catalase on the electrode surfaces have attracted considerable interest due to their advantages in terms of simplicity, short response time, high sensitivity and excellent selectivity [33,45–48]. For immobilization of catalase onto electrode surfaces, different approaches such as physical adsorption, entrapment and encapsulation have been used. However, it is still a challenge for assembling catalase and IL via LBL technique to study the direct electron transfer.

In the present study we report the fabrication, characterization and analytical performance of a H_2O_2 biosensor based on LBL deposition of NH_2-IL and catalase onto titanium nitride nanoparticles modified GC electrode. Direct electrochemistry and electrocatalytic activity of immobilized catalase toward H_2O_2 was investigated. Finally, the applicability of the proposed biosensor for the analysis of H_2O_2 concentration in real samples was demonstrated.

2. Experimental

2.1. Chemical and reagents

Catalase (EC 1.11.1.6) from bovine liver was purchased from Sigma and used without further purification. 5 mg mL^{-1} catalase in phosphate buffer solution (PBS 0.1 M, pH 7) was stored at 4 °C and pure nitrogen was passed through the solution to avoid possible oxygen action during the experiments. The applied amine terminated ionic liquid, 1-(3-Aminopropyl)-3-methylimidazolium bromide (NH_2-IL) was synthesized and characterized (as described in next section). Titanium nitride nanoparticles (TiNnp) with average particle size 20 ± 5 nm and specific surface area of 80 $m^2\ g^{-1}$ were purchased from Plasma Chem GmbH, Germany. Other chemicals with analytical grade were purchased from Sigma or Merck and used without further purification. The milk and bleaching cream as real samples were provided from market and pharmacy.

2.2. Instrumentation

Electrochemical measurements were carried out with a computer-controlled-Autolab modular electrochemical system (Eco Chemie Ultecht, The Netherlands), driven with GPES software (Eco Chemie) with a conventional three-electrode system. A GC electrode modified with TiNnp, NH_2-IL and catalase was used as a working electrode, and a Pt wire and an Ag/AgCl/satd. KCl were employed as auxiliary and reference electrodes, respectively. The effective area of the electrode modified with TiNnp/NH_2-IL was determined as 0.125 cm^2 from cyclic voltammograms of 10 mM $K_4[Fe(CN)_6]$ in buffer solution at pH 7. UV–Vis absorption spectra were recorded with a Carry 1A UV-Vis spectrometer (Perkin-Elmer instruments) on an indium tin oxide (ITO) glass electrode. The surface morphology of modified electrodes was characterized with a Vega-Tesacn electron microscope.

2.3. Synthesis of amine-terminated IL

1-(3-Aminopropyl)-3-methylimidazolium bromide (NH_2-IL) was synthesized based on the procedure reported in the literature [49]. Briefly, 3-bromopropylole amine hydrobromide (0.55 g, 2.5 mmol) and 1-methylimidazole (0.20 mL, 2.5 mmol) were added to 12.5 mL ethanol. The resulting colorless solution was refluxed under nitrogen for 24 h. By recrystallization from ethanol, with ethyl acetate as anti-solvent, the resulting turbid mixture was purified. Finally, the resulting white powder was dried under vacuum at 60 °C overnight. The synthesized IL was characterized by FT-IR technique.

2.4. Preparation of the biosensor

The fabrication of GC/TiNnp/(catalase/NH_2-IL)$_n$ biosensor consists mainly of three steps: In the first step, 5 mg of titanium nitride was dispersed in an aqueous solution (5 mL) and sonicated for 30 min. 10 μL of the slurry was dropped on the GC electrode and dried at the room temperature. In the second step, the GC electrode coated with TiNnp was immersed in 1 mM NH_2-IL and

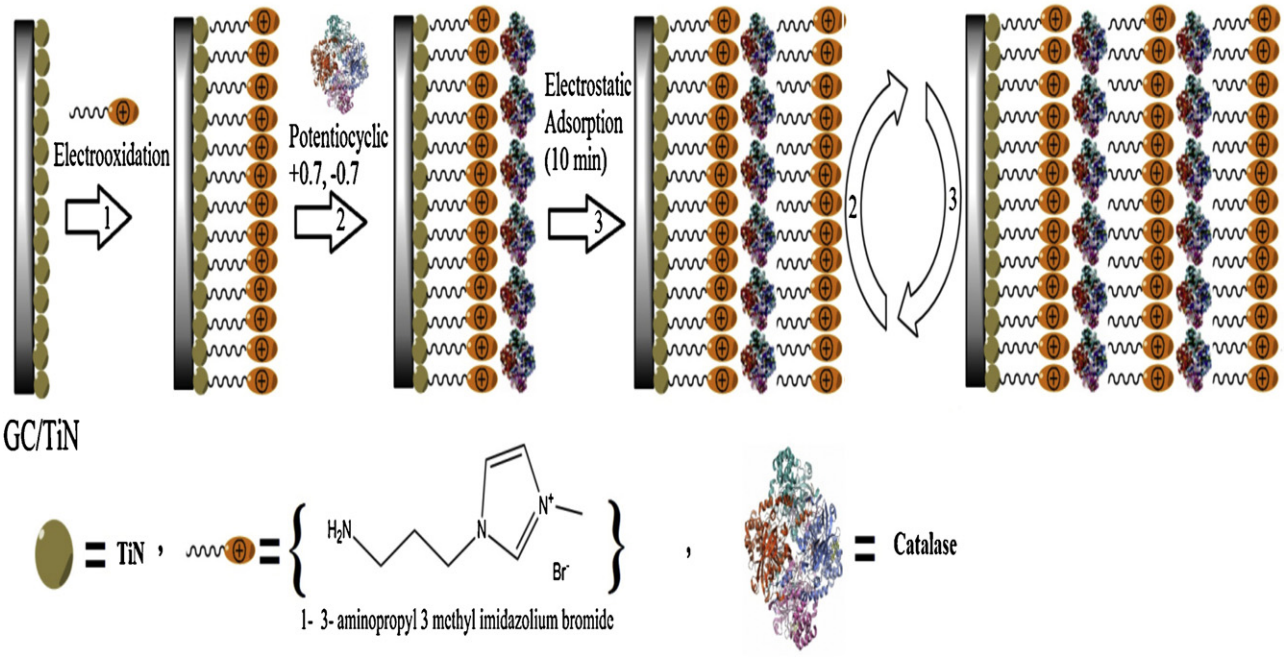

Scheme 1. The stepwise fabrication process of the multilayers film on a GC electrode.

covalent attachment was performed by cycling the potential (15 scans) between 0.0 and 2 V (vs. Ag/AgCl/3 M KCl) at a scan rate of 100 mV s^{-1}. During electro-oxidation of amine group, NH_2-IL is covalenty attached to the surface of TiNnp/GC electrode. The electrochemical oxidation of amino compounds (R-NH_2) grafts organic layer on the electrodes surfaces [50].

In the last step, with immersing GC/TiNnp/NH_2-IL in phosphate buffer solution (PBS, pH 7) containing catalase (1 mg mL^{-1}) and cycling the potential between −0.7 and 0.7 V (10 cycles), catalase was assembled on this novel nanocomposite through ionic interaction and GC/TiNnp/NH_2-IL/catalase was obtained. For formation of GC/TiNnp/NH_2-IL/catalase/NH_2-IL electrode, the second IL layer was assembled through electrostatic interaction between IL with positive charge and catalase with negative charge. These steps were repeated sequentially for $(n-1)$ times and the proposed biosensor $\{(NH_2\text{-IL})\text{–catalase}\}_n$–TiNnp–GC was fabricated. The same procedure was applied for multilayer formation of NH_2-IL/catalase on the ITO electrode. The process of the preparation biosensor based on layer by layer assembly is illustrated in Scheme 1.

3. Results and discussion

3.1. Characterization of nanocomposite and direct electron transfer kinetics of immobilized catalase

In order to investigate the formation of nanocomposite, scanning electron microscopy (SEM) images of GC electrode modified with TiNnp and NH_2-IL before and after applying potential cycling for covalent attachment of IL were recorded (Fig. 1 of supplement). As it can be seen some parts of GC surface was covered with nanocomposite (Fig. 1A of supplement), while after cycling the potential (15 scans between 0.0 and 2.0 V at scan rate 10 mV s^{-1} in PBS, pH 7) a relatively uniform nanocomposite film was immobilized onto GC surface (Fig. 1B of supplement). Furthermore, SEM images of GC/TiNnp and GC/IL/TiNnp/catalase are shown (Fig. 2 of supplement). As illustrated TiNnp with diameter size 20 ± 5 nm and IL-film immobilized onto GC electrode and after entrapment of catalase onto GC/IL/TiNnp a uniform of nanobiocomposite immobilized onto electrode surface. The electrochemical behavior of different electrodes was studied by recording their cyclic voltammograms. Fig. 1 shows cyclic voltammograms obtained for bare GC, GC/TiNnp/NH_2-IL, GC/NH_2-IL/catalase and GC/TiNnp/NH_2-IL/catalase modified electrodes in PBS (pH 7).

As illustrated for GC and GC/TiNnp/NH_2-IL no redox peaks were observed at potential range 0.7 to −0.7 V. However well-defined redox peaks were observed for GC/NH_2-IL/catalase and GC/TiNnp/NH_2-IL/catalase modified electrodes. This result indicates that IL film plays an important role in immobilization and direct electron transfer of the catalase. Therefore, catalase can bind to NH_2-IL through electrostatic–ionic interaction. For immobilized catalase onto IL film well nearly symmetric redox anodic and cathodic peaks at −0.08 and 0.0 V vs. Ag/AgCl were observed. This demonstrates that the presence of IL can facilitate the electron transfer reaction between redox enzyme and electrode. Compared to GC/NH_2-IL/catalase for GC/TiNnp/NH_2-IL/catalase the current response was remarkably enhanced, indicating the addition of TiNnp to the amine-terminated IL film further promotes the electron transfer rate of catalase. Therefore, the integration of TiNnp and NH_2-IL provides a remarkable synergistic effect for direct electron transfer of catalase. In the present study, the effect of IL and TiNnp on direct electron transfer kinetics of catalase was investigated. Cyclic voltammograms of GC/TiNnp/$\{(NH_2\text{-IL})\text{–catalase}\}_7$ modified electrode at different scan rates are shown in Fig. 2. The relationship between peak current and scan rate was found to be linear (Inset "a" of Fig. 2), which indicates surface confined electron transfer process. The peak-to-peak separation is about 100 mV at the scan rate below 100 mV s^{-1}, suggesting facile charge-transfer kinetics over this range of sweep rate. On the other hand, it is found that at the scan rate above of 1 V s^{-1}, ΔEp is increased by increasing the scan rate (inset "b" of Fig. 2). The values of peak-to-peak potential separations are proportional to the logarithm of the scan rate being higher than 2000 mV s^{-1}. According to the Laviron theory, the transfer coefficient (α) and the electron transfer rate constant (k_s) can be estimated by measuring the variation of peak potential

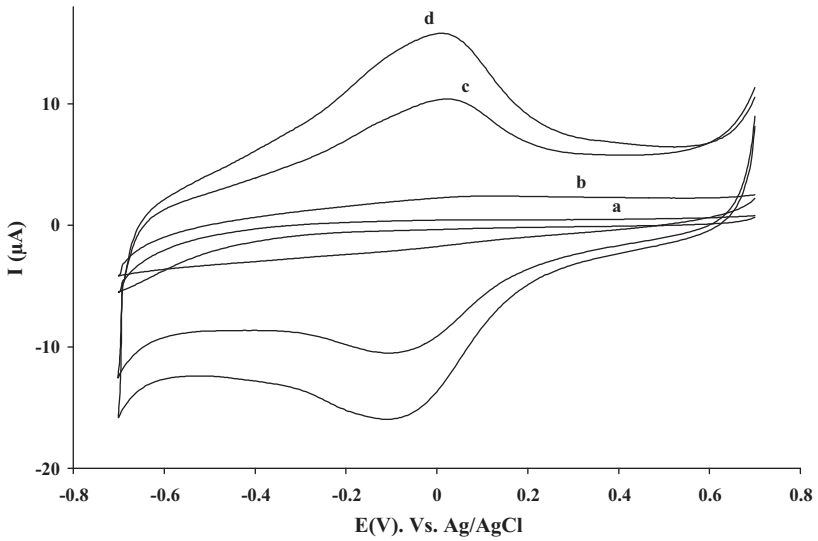

Fig. 1. Cyclic voltammetric response of bare GC electrode (a), GC/TiNnp/NH_2-IL (b), GC/NH_2-IL/catalase (c) and GC/TiNnp/NH_2-IL/catalase (d) in PBS (pH 7) and scan rate 50 mV s^{-1}.

with scan *rate* [51]. The transfer coefficient and heterogeneous electron transfer rate constant are about 0.3 and 5.3 s^{-1}, respectively. This value for the electron transfer rate constant is comparable to or higher than the apparent heterogeneous electron transfer rate constant of catalase at pyrolytic graphite electrode (PGE)/gold nanoparticles (GNP) 1.387 s^{-1} [52], silk fibroin films 0.34 s^{-1} [53], MWCNTs modified GCE 1.07 s^{-1} [54] and nickel oxide nanoparticles 3.7 s^{-1} [47].

The pH of the buffer solution affected the electrochemical behavior of the GC/TiNnp/{(NH_2-IL)–catalase}$_7$ modified electrode. As it is shown (Fig. 3 of supplement), a stable and well-defined redox peak was observed in different pH values, 1–12. Furthermore, both reduction and oxidation peak potentials are shifted toward the negative direction with increasing of the pH values. Quantitative analysis shows that the formal potential ($E^{\circ\prime}$) depends linearly on the pH of solution, with a slope of −64.7 mV pH^{-1} (the correlation coefficient is 0.9982), which is close to the expected value of −58.0 mV pH^{-1} for the one-proton transfer coupled one-electron-transfer reaction, written as:

$$\text{Catalase-HemFe(III)} + H^+ + e^- \rightarrow \text{Catalase-HemFe(II)} \quad (1)$$

3.2. Characterization of the GC/TiNnp–(NH_2-IL/catalase)$_n$ multilayers modified electrode

The build of the multilayer film was assessed by cyclic voltammetry, electrochemical impedance technique, and UV–Vis spectrometery. Fig. 3A shows representative cyclic voltammograms

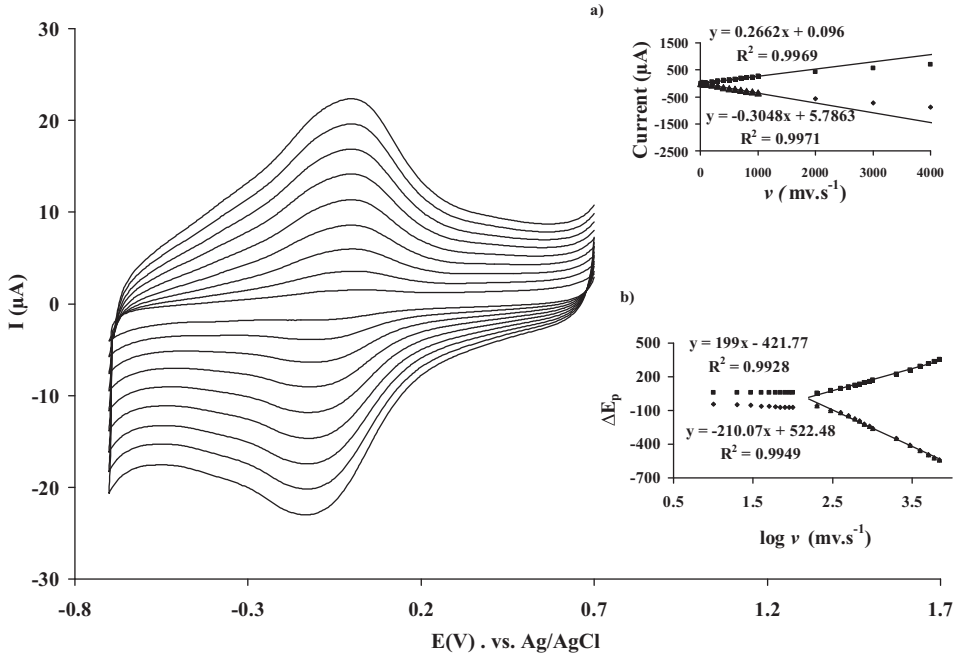

Fig. 2. CVs GC/TiNnp/{(NH_2-IL)–catalase}$_7$ modified electrode at various scan rates in pH 7 PBS, from inner to outer, 10, 20, 30, 40, 50, 60, 70, 80, 90 and 100 mV s^{-1} in pH 7 PBS. Insets: plot of peak currents vs. scan rate (a) and the variation of peak potential separation vs. log υ (b).

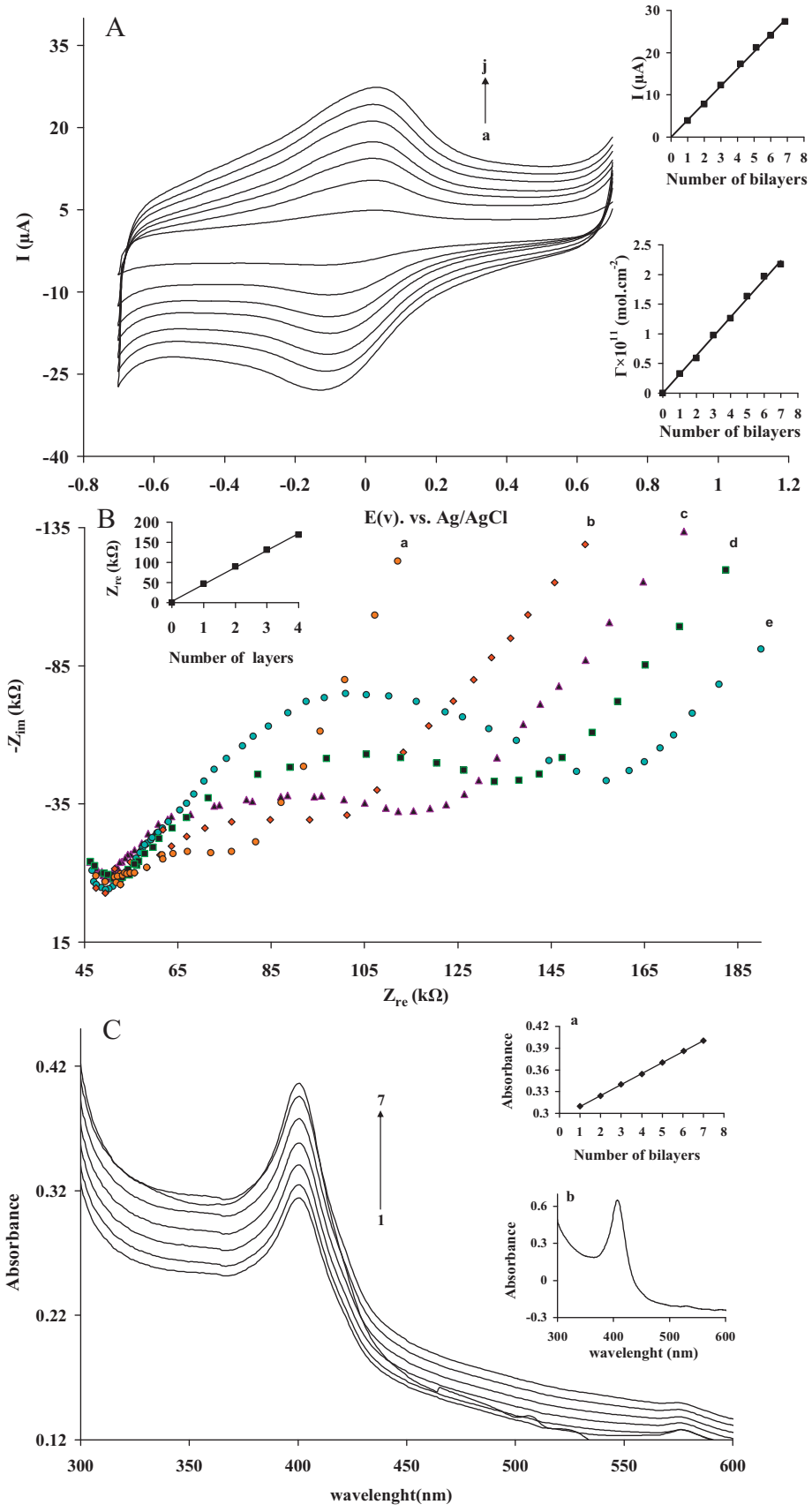

Fig. 3. (A) Cyclic voltammograms of GC/TiNnp/{(NH_2-IL)–catalase}$_n$ with the number of bilayers (n) of 1–7 (from inner to outer) in pH 7 PBS and scan rate 100 mV s^{-1}. Insets: plots of peak current and surface concentration vs. number of bilayer. (B) Nyquist plots of GC (a) and GC/TiNnp/{(NH_2-IL)–catalase}$_n$ with the bilayer number (n) of 1(b), 2(c), 3(d) and 4(e) in pH 7 PBS containing 10 mM of $K_4Fe(CN)_6$ + 10 mM $K_3Fe(CN)_6$ and 0.1 M KCl, inset: relationship between the electron transfer resistance (R_{et}) and the number of bilayers. (C) UV–Vis spectra of ITO/TiNnp/{(NH_2-IL)–catalase}$_7$ modified electrode with the bilayer number (n) of 1–7 (from inner to outer) in pH 7 PBS. Inset (a) plot of absorbance values vs. bilayer number. Inset (b), absorbance spectrum of dissolved catalase in PBS, pH 7.

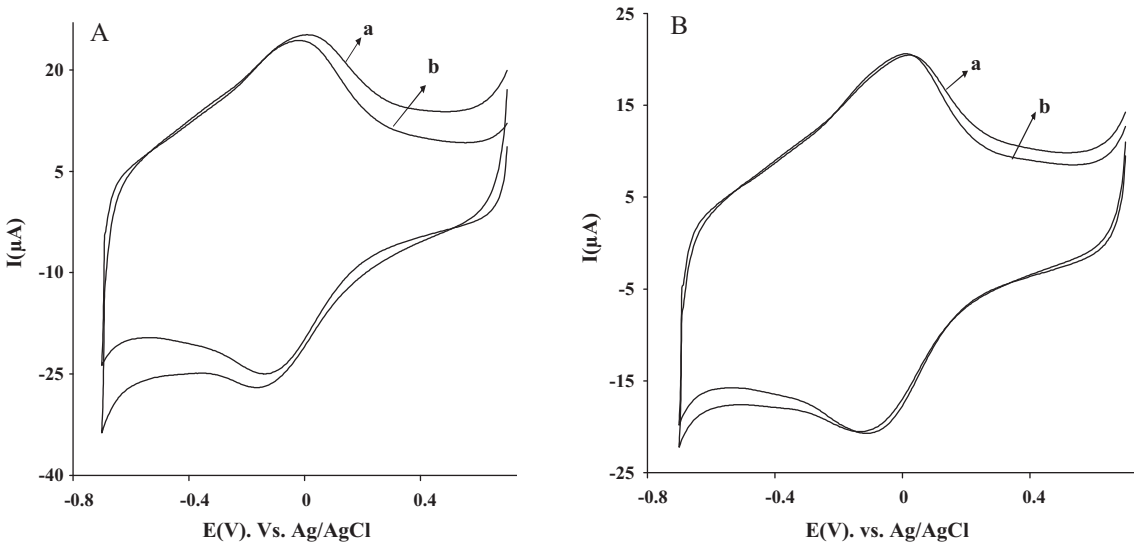

Fig. 4. (A) The 1st (a) and 250th (b) recorded cyclic voltammograms of GC/TiNnp/{(NH_2-IL)–catalase}$_7$. (B) Recorded cyclic voltammograms of the fresh GC/TiNnp/{(NH_2-IL)–catalase}$_7$ modified electrode (a) and after it kept at refrigerator for 7 days (b), electrolyte was PBS pH 7 and scan rate was 100 mV s^{-1}.

for the electrodes made with one to seven bilayers of catalase/NH_2-IL. As it can be seen, by increasing the number of bilayers both reduction and oxidation peak currents are increased regularly. The linear relationship between peak current and bilayer number (inset "a" of Fig. 3A) indicates the same amount of catalase contained in each bilayer. The surface concentration of immobilized catalase (Γ) on the modified electrode for each bilayer was calculated by integration of the cyclic voltammetric curve and based on Faraday's equation, $\Gamma = Q/nFA$. The surface concentration of catalase is 3.5×10^{-12} mol cm^{-2} for GC/TiNnp/(NH_2-IL/catalase)$_1$ and is increased to 7.2, 11, 14.2, 17.5, 20.5 and 23.5×10^{-12} mol cm^{-2} for GC/TiNnp(NH_2-IL/catalase)$_{2-7}$, respectively. Regression analysis of the surface concentration of catalase vs. the number of bilayers (1–7 layers) yielded linear response; Γ (mol cm^{-2}) = 3.32 ($\pm$0.2) $\times 10^{-12}$ [layer number] + 0.61 ($\pm$0.02) $\times 10^{-12}$ (mol cm^{-2}) and R^2 = 0.9978. It can be seen that Γ linearly depends on the number of bilayers and the increment of catalase per NH_2-IL/catalase bilayers is 3.32 ($\pm$0.2) $\times 10^{-12}$ mol cm^{-2}.

Electrochemical impedance spectroscopy (EIS) technique has been proved to be an effective method for probing the features of surface-modified electrodes. This technique has also been successfully used to characterize the formation of multilayer films on different substrates [55]. In the present study, EIS was applied to investigate the LBL deposition of catalase/IL multilayer film on GC/TiNnp electrode. Fig. 3B illustrates the results of the electrochemical impedance studies on GC/TiNnp/{(NH_2-IL)–catalase}$_n$ (n = 1–4) in PBS, pH 7. The bare GC electrode exhibits an almost straight line, which is characteristic of diffusion limited electrochemical process (not shown). After the assembly of TiNnp and NH_2-IL on the electrode surface, a semicircle part of the impedance spectrum (curve "*a*") can be observed, due to the electron transfer resistance of IL-film. When catalase was attached to IL modified GC electrode, the interfacial resistance increased highly (curve "*b*") due to the nonconductive layer of catalase and IL. With increasing the number of layers, the diameters of the semicircles increase. This implies that the interfacial charge transfer becomes more and more difficult and the insulating layer (IL-catalase) on the electrode surface becomes thicker and thicker. On the other hand, as illustrated in the inset of Fig. 3B a good linear relationship between R_{et} and layer number is observed. These results indicate that NH_2-IL/catalase multilayer films can be formed uniformly on TiNnp/GC electrode.

UV–Vis spectroscopy is performed to characterize the deposition and to build up the catalase-IL multilayer films. Since the adsorption intensity is proportional to the concentration of the deposited material, the structure of LBL films can be estimated. Fig. 3C shows the absorption spectra of multilayer films {NH_2-IL/catalase}$_n$ with different number of bilayers, n = 1–7 on the ITO electrode. The {NH_2-IL/catalase}$_n$ films exhibit a soret absorption band at 402 nm. For catalase in pH 7 phosphate buffer solution the absorption band at the same wavelength was observed (inset "b" of Fig. 3C). These results indicate that no observable denaturation of catalase is found when it was immobilized onto TiNnp/IL film. The same absorption band has been observed for catalase incorporated in nickel oxide nanoparticles [47] and polyacrylamide hydrogel film [56]. Furthermore, it can be seen that the absorption of catalase/NH_2-IL multilayer films occurs at the same wavelength with sequential immobilization. The linear increase of the intensity of the absorption peak as a function of layers number (inset "a" of Fig. 3C) indicates that regular and uniform catalase/NH_2-IL film has been successfully assembled layer-by-layer.

3.3. *Stability of the GC/TiNnp/{(NH_2-IL–catalase}$_n$ modified electrode*

Long term stability is one of the most important properties of sensors, biosensors and bioreactors. The stability of GC/TiNnp/{(NH_2-IL–catalase}$_7$ modified electrode was investigated by recording cyclic voltammograms and monitoring the remaining amount of active substance after successive sweeps of potential cycling. The peak height and peak potential of immobilized film remained nearly unchanged and the amount of catalase left on the electrode surface was almost 95% of its initial value after 250 successive cycles in electrolyte solution with a scan rate of 100 mV s^{-1} (Fig. 4A). In addition, no significant decrease can be seen after replacing the electrolyte having been used for 250 repetitive cycles with fresh solution. The stability of the modified film was investigated by recording cyclic voltammogram of GC/TiNnp/{(NH_2-IL–catalase}$_7$ electrode in buffer solution (pH 7), after storing it in a refrigerator (4 °C) for 7 days showing excellent storage stability of the chemically modified electrode. The CV peak potentials remained at the same position and the reduction peak currents were decreased by only about 4% (Fig. 4B). Thus, high stability of the modified electrode is related to the chemical

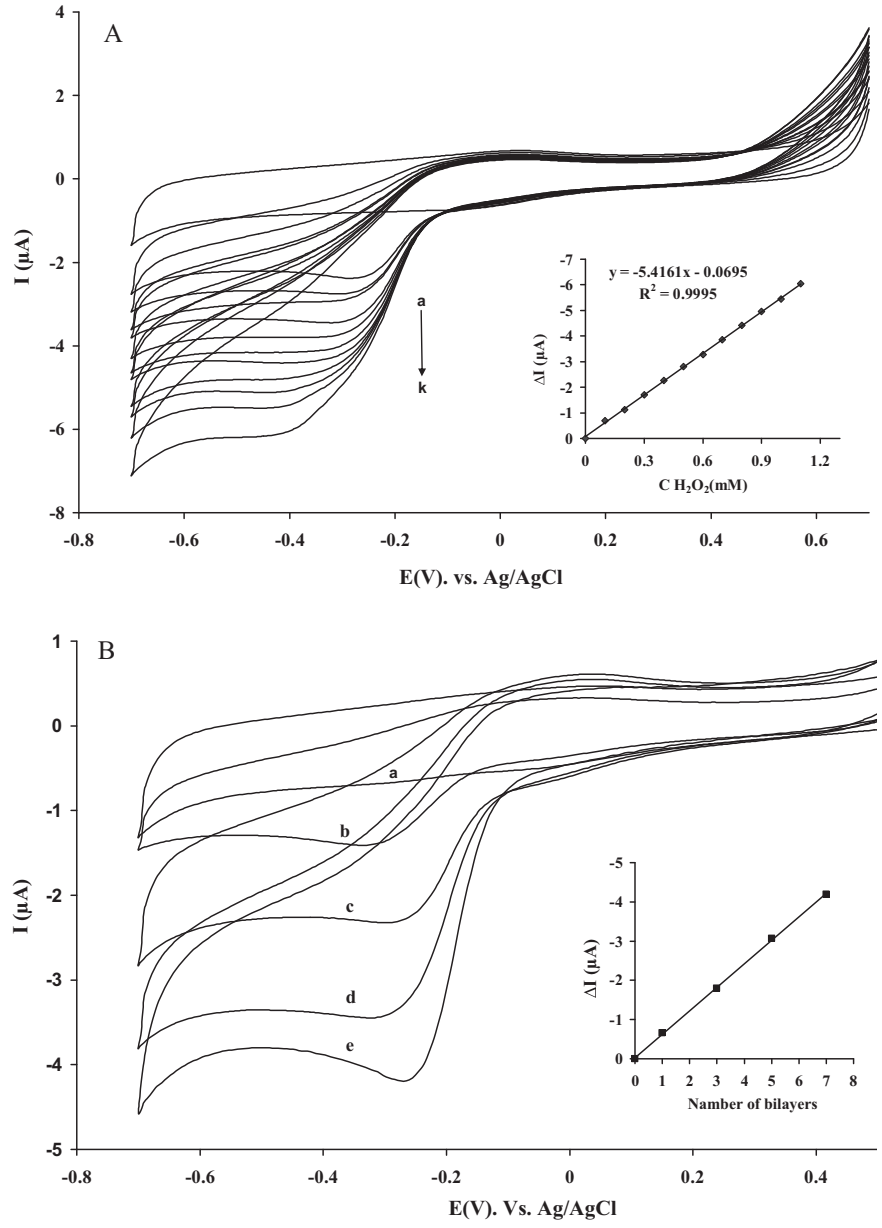

Fig. 5. (A) CVs of GC/TiNnp/{(NH2-IL)–catalase}$_7$ modified electrode in the presence of different concentrations of H_2O_2 from inner to outer 0.1, 0.2, 0.3, 0.4, 0.5, 0.6, 0.7, 0.8, 0.9, 1 and 1.1 mM in PBS (pH 7) and scan rate 20 mV s^{-1}. Inset: the catalytic current response vs. H_2O_2 concentrations. (B) Cyclic voltammograms of the GC/TiNnp/{(NH_2-IL)–catalase}$_n$ modified electrode with the bilayer number (b) 1, (c) 3, (d) 5 and (e) 7 in the presence of 0.4 mM H_2O_2. (a) Cyclic voltammogram of GC/TiNnp/(NH_2-IL)–catalase modified electrode in the absence of H_2O_2, in the same measurement condition. Inset: plot of catalytic current response vs. bilayers number.

stability of nanocomposite film, the interaction between catalase and IL strong adsorption of catalase on nanocomposite. Therefore, the GC/TiNnp/{(NH_2-IL–catalase}$_7$ modified electrode can be used as a biosensor due to its long term stability and excellent electron transfer rate constant.

3.4. Electrocatalytic reduction of H_2O_2 at GC/TiNnp/NH_2-IL–catalase modified electrode

It has been reported that proteins and enzymes containing the heme group such as horseradish peroxides, cytochrome C, hemoglobin and catalase have the ability to reduce H_2O_2 and O_2 electrocatalytically [57–63]. In this research electrocatalytic activity of the modified electrode toward reduction of hydrogen peroxide was examined using cyclic voltammetry technique. Fig. 5A shows the cyclic voltammetric response of GC/TiNnp/(NH_2-IL–catalase)$_7$ modified electrode to H_2O_2 reduction. As it is illustrated, the peak current is linearly increased with increasing H_2O_2 concentration. The linear regression equation for the concentration ranged from 0.1 to 1.1 mM was I (μA) = 5.416 (±0.300) [H_2O_2] mM − 0.0695 (±0.0040) (μA), R^2 = 0.9995. The detection limit is estimated to be 10 μM when the signal to noise ratio is 3.

The LBL assembly process toward formation of bilayers of catalase/NH_2-IL film onto GC/TiNnp electrode was also confirmed by electrocatalytic reduction of H_2O_2. Fig. 5B shows the cyclic voltammetric responses of GC–TiNnp electrode modified with different numbers of catalase/NH_2-IL bilayers in the presence of 0.4 mM H_2O_2. As it can be seen, the current response increases with increasing the number of assembled NH_2-IL/catalase bilayers (voltammograms b–f), up to at least 7 (inset of Fig. 5B). These results indicate that every bilayer contains the same amount of

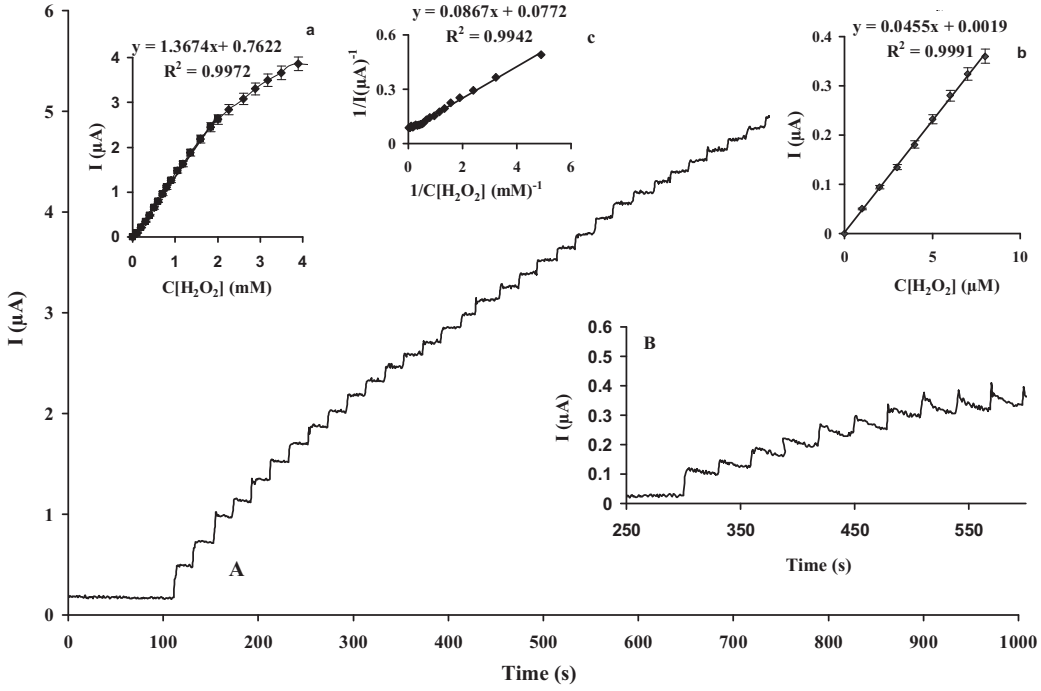

Fig. 6. Amperometric response of GC/TiNnp/{(NH_2-IL)–catalase}$_7$ modified electrode during successive addition (A) 0.1 mM and (B) 1 μM: conditions −0.35 V constant potential in pH 7 PBS and rotation speed 2000 rpm. Insets (a and b) plots of chronoamperometric current vs. H_2O_2 concentration and linear calibration curve for determination of K_M (plot c).

active enzyme and also shows the regular growing of the multilayer assembly.

3.5. Amperometric response of GC/TiNnp/NH_2-IL/catalase modified electrode

Fig. 6 illustrates a typical current–time plot for the GC/TiNnp/(NH_2-IL–catalase)$_7$ biosensor upon the successive addition of H_2O_2 at −0.35 V. As it is shown with addition of 0.1 mM (chronoamperogram A) and 1 μM (chronoamperogram B) of H_2O_2, the biosensor exhibits excellent response. The current response of the biosensor is increased with increasing H_2O_2 concentration. The enzyme electrode reached 95% of the steady state current within 10 s. The enzyme electrode gave a linear response to H_2O_2 in the range from 1.0 μM to 2.1 mM. The calibration plot over the concentration range of 1–8 μM has a slope of 380 μA mM^{-1} cm^{-2} (sensitivity), correlation coefficient of 0.9991 and detection limit of 100 nM at the signal-to-noise ratio of 3. These results are promising and indicate that the biosensor possesses high biological affinity for H_2O_2. These analytical parameters are better than or at least comparable with other catalase based H_2O_2 biosensors (Table 1).

The sensitivity of biosensor is directly correlated to the number of assembled bilayers of IL-catalase, indicating the ability of the procedure to control the sensitivity of the enzyme-based modified electrode. When the concentration of H_2O_2 was higher than 2 mM, a response plateau was observed, showing the

Table 1
Analytical parameters of different H_2O_2 biosensors.

Modified electrode	Linear range (mM)	Sensitivity (μA mM^{-1} cm^{-2})	Detection limit (nM)	Γ ($\times 10^{-11}$ Mol cm^{-2})	k_s (s^{-1})	K_M (mM)	Ref.
CAT[1]–PAM[2]	0.4–0.8	–	–	2.36	29	–	[56]
CAT-MC[3]	0.02–0.12	32	2500	2.36	2.9	–	[65]
CAT-SF[4]	0.003–0.158	940	–	6.27	0.337	–	[53]
CAT-PNM[5]	0.002–0.035	2.9	–	1.43	17	–	[66]
CAT/cysteine/Si sol–gel	0.001–0.03	16.1	400	–	4.8	–	[67]
CAT-agarose	0.001–0.818	2.17	–	2.99	49.1	31.7	[68]
CAT-SWCNTs[6]	0.7–1.1	–	4000			–	[62]
CAT-MWCNTs	0.01–0.1	3.3	4000	2.4	80	1.7	[45]
NF-MWCNTs–CAT-AuNPs[7]	1–5		–	–	1.387	–	[69]
CAT-NiO[8]	0.001–1.0	15.9	600	–	3.7	0.96	[47]
GCE/Graphen-NH_2/AuNPs/CAT	3×10^{-4} to 0.6	13.4	50	0.333	2.34	2.81	[70]
Sol–gel/chitosan/HRP[9]	5×10^{-6} to 1×10^{-4}	–	2	–	–	1.30×10^{-3}	[71]
GC/MWCNTs/[bmim][PF6][10]/CAT	5×10^{-6} to 1.7×10^{-3}	–	0.25	0.309	1.95	–	[72]
GC/AuNP-GO[11]/TCA[12]	10^{-4} to 2.3	–	10	–	–	0.98	[73]
GC/MWCNTs/NiO/CAT	0.20–2.53	337.58	19×10^3	0.153	1.6	1.68	[74]
SWCNT/HRP	–	1.79×10^{-4}	40	8	–	–	[75]
GC/NF/CAT/ERGO[13]	0.05–1.91	7.76	–	95.1	–	–	[76]
HRP/Phz[14]	2×10^{-6} to 10^{-2}	900	1	–	–	–	[77]
GC/TiNnp/(catalase-IL)$_7$ electrode	0.001–2.1	380	100 nM	35	5.28	1.1	This work

1 – catalase; 2 – polyacrylammide; 3 – methyl cellulose; 4 – silk fibroin; 5 – poly(N-isopropylacrylamide-co-3-methacryloxypropyltrimethoxysilane); 6 – single-wall carbon nanotubes; 7 – gold nanoparticles; 8 – nickel oxide; 9 – horseradish peroxidase; 10 – 1-butyl-3-methylimidazolium hexafluorophosphate; 11 – graphene oxide; 12 – thionine-conjugated catalase enzyme; 13 – electrochemically reduced graphene oxide; 14 – phenothiazine.

Table 2
Determination of H_2O_2 in real samples using GC/TiNnp/IL/catalase modified electrode.

Sample no.	Spiked μM	Found μM	Recovery (%)
1 (milk)	0.00	5.52(±0.20)	–
	10	15.96 (±0.40)[a]	102.86 (±2.5)
2 (bleaching cream)	0.0	58.77 (±0.60)	–
	10.0	67.97 (±0.70)	98.83% (±1.30)

[a] The mean value for three measurements.

characteristics of the Michaelis–Menten kinetic mechanism. The apparent Michaelis–Menten constant (K_M), which gives an indication of the enzyme–substrate kinetics, can be obtained from the Lineweaver–Burk equation [64],

$$\frac{1}{I_{ss}} = \frac{1}{I_{max}} + \frac{K_M}{I_{max}} \cdot \frac{1}{C} \quad (2)$$

where I_{ss} is the steady-state current after the addition of substrate, C is the bulk concentration of the substrate and I_{max} is the maximum current measured under saturated substrate solution. K_M can be obtained by the analysis of the slope and intercept of the plot of the reciprocals of the steady state current vs. H_2O_2 concentration. The Michaelis–Menten constant of the system (K_M) in this work was found to be 1.1 (±0.1) mM, implying that the GC/TiNnp/{(NH_2-IL)–catalase}$_7$ modified electrode exhibits a high affinity for H_2O_2. Also the stability of GC/TiNnp/{(NH_2-IL)–catalase}$_7$ modified electrode has been checked by monitoring the amperometric response of 4 μM H_2O_2 for a period of 1000 s (Fig. 4 of supplement). It has been found that the biosensor retained 97% of current response after 17 min. The good stability is attributed to the following aspects: the fabrication process is mild, no damage is made on the enzyme molecules, and the interaction is strongly among IL, catalase and TiNnp. Finally, the good biocompatibility of IL maintains the biological activity of the enzyme immobilized on the electrode.

3.6. Determination of H_2O_2 in real samples

In order to estimate the applicability of the methodology, the modified electrode was tested by applying it to the measurement of H_2O_2 concentration in real samples. In this case the proposed biosensor was applied to the measurement of H_2O_2 concentration in real samples (milk and bleaching cream). The milk sample diluted 9 times with 0.2 M, PBS (pH 7) prior to measurements. The cream sample was provided from pharmacy and 1 mL of it dissolved in PBS (pH 7) and after filtration it can be used for measurements. The standard addition method was adopted to demonstrate the possibility of H_2O_2 detection in real samples. The obtained results were given in Table 2. It could be seen that there is a good agreement between the spiked and found values for detection of H_2O_2l. These results clearly indicate that the system presented in this work is valid for the analysis of H_2O_2 in real samples.

4. Conclusion

In summary, for the first time a multilayer film of catalase and amine-terminated IL was successfully immobilized onto GC/TiNnp by layer by layer assembly method based on the electrostatic attraction between positively charged IL and negatively charged catalase. Combining the advantages of LBL assembly technique and IL based nanocomposite improve biosensor characteristics such as minimizing protein denaturation and controlling of film thickness. The linear and regular growth of the multilayer film was characterized by cyclic voltammetry, electrochemical impedance, and UV–Vis spectroscopy techniques. The {(NH_2-IL–catalase}$_n$–TiNnp–GC electrode demonstrated a well defined direct CV response, for redox couple of catalase with electron transfer rate constant (k_s) of 5.28 s^{-1}. The proposed biosensor showed excellent electrocatalytic activity toward H_2O_2 reduction and the catalytic response was enhanced significantly by increasing the number of bilayers, which indicated that the sensitivity was tunable by controlling the film thickness. At concentration range up to 2.1 mM, the detection limit and sensitivity of the proposed biosensor toward H_2O_2 reduction were 100 nM and 380 μA mM^{-1} cm^{-2}, respectively. These results indicated that the proposed layer by layer technique is a very interesting method for the preparation of bionanostructures with high molecular order. Due to synergic effects of IL, TiNnp and catalase, the proposed biosensor exhibits excellent performance such as high reproducibility, storage stability, short response time and wide linear range in comparison to other catalase-based H_2O_2 biosensors. The prepared bionanostructures can be applied for the fabrication of the effective third generation biosensors, biofuel cells and bioelectronics devices.

Acknowledgments

The financial supports of the Iranian Nanotechnology Initiative and the Research Office of the University of Kurdistan are gratefully acknowledged. Authors also thank Dr. Arash Sorori for his valuable comments.

Appendix A. Supplementary data

Supplementary data associated with this article can be found, in the online version, at http://dx.doi.org/10.1016/j.aca.2012.09.043.

References

[1] J. Yu, T. Zhao, F. Zhao, B. Zeng, Electrochim. Acta 53 (2008) 5760–5765.
[2] J. Li, X. Lin, Biosens. Bioelectron. 22 (2007) 2898–2905.
[3] K.M. Manesh, P. Santhosh, A. Gopalan, K.P. Lee, Talanta 75 (2008) 1307–1314.
[4] E.J. Calvo, C. Danilowicz, R. Etchenique, L. Pietrasanta, A. Wolosiuk, Anal. Chem. 73 (2001) 1161–1168.
[5] M. Ferreira, P.A. Fiorito, O.N. Oliviera Jr., S.I. Córdoba De Torresi, Biosens. Bioelectron. 19 (2004) 1611–1615.
[6] N. Ferreyra, L. Coche-Guérente, P. Labbe, Electrochim. Acta 49 (2004) 477–484.
[7] R.M. Iost, F.N. Crespilho, Biosens. Bioelectron. 31 (2012) 1–10.
[8] J.B. Schlenoff, Langmuir 25 (2009) 14007–14010.
[9] Q. Zhang, S. Wu, L. Zhang, J. Lu, F. Verproot, Y. Liu, Z. Xing, J. Li, X.M. Song, Biosens. Bioelectron. 26 (2011) 2632–2637.
[10] Y.J. Shin, S.H. Kim, D.H. Yang, H. Kwon, J.S. Shin, J. Ind. Eng. Chem. 16 (2010) 380–384.
[11] M. Pellissier, F. Barriere, A.J. Downard, D. Leech, Electrochem. Commun. 10 (2008) 835–838.
[12] Y. Sun, H. Wang, C. Sun, Biosens. Bioelectron. 24 (2008) 22–28.
[13] A. Salimi, A. Noorbakhsh, Electrochim. Acta 56 (2011) 6097–6105.
[14] S. Ghosh, J. Chem. Res., Synop. 4 (2004) 241–246.
[15] G.J. Zhou, G. Wang, J.J. Xu, H.Y. Chen, Sens. Actuators B 81 (2002) 334–339.
[16] B.K. Cho, H.J. Cho, H. Yun, B.G. Kim, J. Mol. Catal. B: Enzym. 26 (2003) 273–285.
[17] E. Katz, I. Willner, Angew. Chem. Int. Ed. 43 (2004) 6042–6108.
[18] H. Liu, J.F. Rusling, N. Hu, Langmuir 20 (2004) 10700–10705.
[19] N. Maleki, A. Safavi, F. Tajabadi, Anal. Chem. 78 (2006) 3820–3826.
[20] W. Sun, X. Li, Y. Wang, R. Zhao, K. Jiao, Electrochim. Acta 54 (2009) 4141–4148.
[21] J.Y. Sun, K.J. Huang, S.F. Zhao, Y. Fan, Z.W. Wu, Bioelectrochemistry 82 (2011) 125–130.
[22] N.V. Shvedene, D.V. Chernyshov, I.V. Pletnev, Russ. J. Gen. Chem. 78 (2008) 2507–2520.

[23] H. Xu, H.Y. Xiong, Q.X. Zeng, L. Jia, Y. Wang, S.F. Wang, Electrochem. Commun. 11 (2009) 286–289.
[24] S. Wie, W. Dandan, G. Ruifang, J. Kui, Electrochem. Commun. 9 (2007) 1159–1164.
[25] W. Wei, H.H. Jin, G.C. Zhao, Microchim. Acta 164 (2009) 167–171.
[26] H. Sun, J. Porous Mater. 13 (2006) 393–397.
[27] X. Lu, Q. Zhang, L. Zhang, J. Li, Electrochem. Commun. 8 (2006) 874–878.
[28] D. Jia, J. Dai, H. Yuan, L. Lei, D. Xiao, Talanta 85 (2011) 2344–2351.
[29] D. Wei, A. Ivaska, Anal. Chim. Acta 607 (2008) 126–135.
[30] Y. Zhang, R. Yan, F. Zhao, B. Zeng, Colloid Surf. B: Biointerfaces 71 (2009) 288–292.
[31] W. Sun, P. Qin, R. Zhao, K. Jiao, Talanta 80 (2010) 2177–2181.
[32] W.L. Zhu, Y. Zhou, J.R. Zhang, Talanta 80 (2009) 224–230.
[33] P. Rahimi, H.A. Rafiee-Pour, H. Ghourchian, P. Norpuzi, M.R. Ganjali, Biosens. Bioelectron. 25 (2010) 1301–1306.
[34] X. Wu, F. Zhao, J.R. Varcoe, A.E. Thumser, C. Avignone-Rossa, R.C.T. Slade, Bioelectrochemistry 77 (2009) 64–68.
[35] Q.L. Sheng, J.B. Zheng, X.D. Shang-Guan, W.H. Lin, Y.Y. Li, R.X. Liu, Electrochim. Acta 55 (2010) 3185–3191.
[36] K. Liu, J. Zhang, G. Yang, C. Wang, J.J. Zhu, Electrochem. Commun. 12 (2010) 402–405.
[37] T. Zhan, M. Xi, Y. Wang, W. Sun, W. Hou, J. Colloid Interface Sci. 346 (2010) 188–193.
[38] W. Sun, D. Wang, G. Li, Z. Zhai, R. Zhao, K. Jiao, Electrochim. Acta 53 (2008) 8217–8221.
[39] R. Gao, J. Zheng, Electrochem. Commun. 11 (2009) 608–611.
[40] C.N. Kirchner, K.H. Hallmeier, R. Szargan, T. Raschke, C. Radehaus, G. Wittstock, Electroanalysis 19 (2007) 1023–1031.
[41] Y. Wang, H. Yuan, X. Lu, Z. Zhou, D. Xiao, Electroanalysis 18 (2006) 1493–1498.
[42] B. Bas, R. Piech, M. Ziemnicka, W. Reczynski, M. Robotka, Electroanalysis 21 (2009) 1773–1780.
[43] S. Kaskel, K. Schlichte, T. Kratzke, J. Mol. Catal. A 208 (2004) 291–298.
[44] J.H. Bang, K.S. Suslick, Adv. Mater. 21 (2009) 3186–3190.
[45] A. Salimi, A. Noorbakhsh, M. Ghadermarz, Anal. Biochem. 344 (2005) 16–24.
[46] A. Salimi, E. Sharifi, A. Noorbakhsh, S. Soltanian, Electrochem. Commun. 8 (2006) 1499–1508.
[47] A. Salimi, E. Sharifi, A. Noorbakhsh, S. Soltanian, Biophys. Chem. 125 (2007) 540–548.
[48] P.A. Prakash, U. Yogeswaran, S.M. Chen, Sensors 9 (2009) 1821–1844.
[49] Z. Wang, Q. Zhang, D. Kuehnera, X. Xu, A. Ivaska, L. Niu, Carbon 46 (2008) 1687–1692.
[50] J. Ghelani, P. Martin, H. Randrimahazaka, J.C. Lacroix, Electrochem. Commun. 12 (2010) 246–249.
[51] E. Laviron, J. Electroanal. Chem. 101 (1979) 19–28.
[52] B. Zhang, Z. Zhang, B. Wang, J. Yan, J. Li, S.M. Cai, Acta Chim. Sin. 59 (2001) 1932–1936.
[53] Y. Wu, Q. Shen, S. Hu, Anal. Chim. Acta 558 (2006) 179–186.
[54] H. Zhou, T.H. Lu, H.X. Shi, Z.H. Dai, X.H. Huang, J. Electroanal. Chem. 612 (2008) 173–178.
[55] L. Luo, J. Liu, Z. Wang, X. Yang, S. Dong, E. Wang, Biophys. Chem. 94 (2001) 11–22.
[56] H. Lu, Z. Li, N. Hu, Biophys. Chem. 104 (2003) 623–632.
[57] S. Yang, Y. Li, X. Jiang, Z. Chen, X. Lin, Sens. Actuators B 114 (2006) 774–780.
[58] S. Chen, R. Yuan, Y. Chai, L. Xu, N. Wang, X. Li, L. Zhang, Electroanalysis 18 (2006) 471–477.
[59] H. Zhou, X. Gan, J. Wang, X. Zhu, G. Li, Anal. Chem. 77 (2005) 6102–6104.
[60] S. George, H.K. Lee, J. Phys. Chem. B 113 (2009) 15445–15454.
[61] G. Shi, Z. Sun, M. Liu, L. Zhang, Y. Liu, Y. Qu, L. Jin, Anal. Chem. 79 (2007) 3581–3589.
[62] L. Wang, J. Wang, F. Zhou, Electroanalysis 16 (2004) 627–632.
[63] C. Chuang, L. Luo, M. Chang, J. Shih, J. Chin. Chem. Soc. 56 (2009) 771–777.
[64] J. Li, S.N. Tan, H. Ge, Anal. Chim. Acta 335 (1996) 137–145.
[65] Y.M. Li, X.T. Chen, J. Li, H.H. Liu, Electrochim. Acta 49 (2004) 3195–3200.
[66] S.F. Wang, T. Chen, Z.L. Zhang, D.W. Pang, K.L. Wong, Electrochem. Commun. 9 (2007) 1709–1714.
[67] J. Di, M. Zhang, K. Yao, S. Bi, Biosens. Bioelectron. 22 (2006) 247–252.
[68] H. Okuma, E. Watanabe, Biosens. Bioelectron. 17 (2002) 367–372.
[69] B. Zhou, J. Wang, X. Gao, Anal. Lett. 41 (2008) 1832–1849.
[70] K. Huang, D.J. Niu, X. Liu, Z.W. Wu, Y. Fan, Y.-F. Chang, Y.Y. Wu, Electrochim. Acta 56 (2011) 2947–3295.
[71] G. Wang, J.J. Xu, H.Y. Chen, Z.H. Lu, Biosens. Bioelectron. 18 (2003) 335–343.
[72] M. Shamsipur, M. Asgari, M.G. Maragheh, A.A. Moosavi-Movahedi, Bioelectrochemistry 83 (2012) 31–37.
[73] B. Zhang, Y. Cui, H. Chen, B. Liu, G. Chen, D. Tang, Electroanalysis 23 (2011) 1821–1829.
[74] M. Shamsipur, M. Asgari, M.F. Mousavi, R. Davarkhah, Electroanalysis 24 (2012) 357–367.
[75] X. Yu, S.N. Kim, F. Papadimitrakopoulos, J.F. Rusling, Mol. BioSyst. 1 (2005) 70–78.
[76] S.W. Ting, A.P. Periasamy, S.-M. Chen, R. Saraswathi, Int. J. Electrochem. Sci. 6 (2011) 4438–4453.
[77] S.S. Razola, E. Aktas, J.C. Vire, J.M. Kauffmann, Analyst 125 (2000) 79–85.